Trend turning of North China summer extreme precipitations around early 2000s and its possible reason

Yina Diao (diaoyn@ouc.edu.cn)
Ocean University of China College of Oceanic and Atmospheric Sciences https://orcid.org/0000-0002-9035-0439

Jinhuan Guo
Ocean University of China College of Oceanic and Atmospheric Sciences

Yazhou Zhang
Ocean University of China College of Oceanic and Atmospheric Sciences

Zhaolu Hou
Ocean University of China College of Oceanic and Atmospheric Sciences

Research Article

Keywords: North China extreme precipitation, Ural blocking, Western Pacific Subtropical High, trend turning

Posted Date: March 28th, 2023

DOI: https://doi.org/10.21203/rs.3.rs-2720555/v1

Version of Record: A version of this preprint was published at Climate Dynamics on July 6th, 2023. See the published version at https://doi.org/10.1007/s00382-023-06860-1.

Abstract

This study focuses on regional extreme precipitation (REP) in North China. We found a trend turning in summer (July and August) REP frequencies and intensities from a decrease trend in 1961–2002 to an increase trend in 2003–2020, accompanied by a southward shift of the extreme rain belt, and an enhanced connection with the Ural blocking and the Western Pacific Subtropical High Pressure (WPSH) in 2003–2020. Rains in North China are accompanied by a west-east low-high dipole (LHD) at upper troposphere. During the REP, the high of the LHD at Northeast China (the NEH) is strongly amplified from a pre-existing stationary ridge at northeast Asia under the influence of eastward propagating Rossby wave energies along the subpolar/subtropical wave guide over Eurasia. For the REP years, an enhanced stationary ridge over the Ural Mountains in the period 2003–2020 replaces the stationary Ural trough in the period 1961–2002, favouring the development of Ural Blockings (UB) and leading to a change of the Rossby wave propagation path from along the subtropical wave guide in 1961–2002 to along the polar wave guide in 2003–2020. Therefore, a connection between the NEH and the UB forms, which may lead to a higher probability of extreme precipitation in North China since blocking is a major source of strong circulation anomalies. The mean summer WPSH expands more westward-northward in 2003–2020 than in 1961–2002, providing the background conditions for further westward-northward expanding of the daily WPSH under the influence of the NEH before the REP day leading to strong moisture transport from north Pacific and increased intensity and probability of extreme precipitation over southern North China.

1 Introduction

North China is at the north edge of the East Asian summer monsoon (EASM). Summer rains in North China occur at the third stage of seasonal march of the East Asian summer monsoon. For rains in north China, the EASM brings major water vapor. Annual precipitations, especially extreme precipitations in North China, are mainly concentrated in the late summer from July to August (Ding and Chan 2005; Wang et al. 2015; Zhou et al. 2020). As in the northern rain belt of EASM, precipitations in North China is also influenced by the mid-latitude circulations and the western North Pacific subtropical high (WPSH) (Zhang 1999; Li and Zeng 2003; Ding and Chan 2005; Huang et al. 2006; Liu and Ding 2011). Atmospheric blocking events significantly affect the distribution of rainfall over all Eurasian regions in summer (Antokhina et al. 2016) and have an impact on the intraseasonal variability of summer monsoon rainfall in China (Ding and Chan 2005). Precipitations over North China was found to be also connected to two dominant wave trains over summer Eurasian continent, the wave train along the subtropical Asian jet and the wave train pattern along the polar front (Enomoto 2004; Ding and Wang 2005, 2007; Kosaka et al. 2009; Zhu et al. 2011; Schubert et al. 2014). They also have an impact on the intraseasonal variability of precipitations over north China (Gao et al. 2022). Moreover, the subtropical wave train is a bridge between tropical intraseasonal oscillation and North China rainfall (Gao et al. 2022), and the subpolar one is a bridge between Arctic sea ice variability and East China rainfall (He et al. 2018).

Though summer precipitation in North China is much less than that in south China and east China, extreme precipitation can lead to destructive impacts on society (Zhu and Xue 2016). Under a

background of southern-flooding-northern-drought pattern over China in the last decades (Wang 2001; Yu et al. 2004), less attentions are paid to extreme precipitations in North China. The weakening of the EASM circulation since the end of the 1970s (Yu et al. 2004; Yu and Zhou 2007; Zhou et al. 2009) leads to a drying tendency in North China (Zhou et al. 2009, Xu et al. 2015; He et al. 2021). However, Zhou et al. (2013) pointed out that the 2012 flood in North China occurred in the context of a multidecadal drying tendency. Li et al. (2013) found that the summer extreme precipitation in North China showed an increasing trend in the early 21st century. Zhao et al. (2019) found that frequency of extreme precipitation increased from 1997 to 2016 over the North China Plain. In recent years, more attentions have been paid to the topic. Extreme precipitation in North China was found to be related to the westward extension and northward lift of the WPSH (Zhao et al. 2019; Han et al. 2020). Due to its intraseasonal variation, the two Eurasian wavetrains also play an important role in causing extreme precipitation in North China (Orsolini et al. 2015; Han et al. 2021). Yang et al. (2021) further pointed out that heavy precipitations over North China are connected to anomalous anticyclone over the Korean Peninsula conveying more moisture from the North Pacific.

On the other hand, the intensity of the WPSH increases significantly in the 21st century (Gong and He 2002; Zhou et al. 2009; Matsumura et al. 2015; Choi and Kim 2019; Fu and Guo 2020). The strengthening and westward expansion of the WPSH leads to significantly positive correlation between summer rainfall in North China and the WPSH after 1990 (Gao et al. 2014). Due to Arctic warming, sea ice has decreased rapidly (Kwok et al. 2009; Maslanik et al. 2011) since the beginning of 21st century, which was found to have an important impact on rainfall in east Asia through its impacts on mid-latitude circulations (Nakamura and Sato 2022; He et al. 2018). Liu et al. (2022) pointed out that positive summer shortwave cloud radiative anomalies over northern Russia favor the generation of the Ural blocking, and trigger the positive Eurasian pattern, resulting in an increase of precipitation in northern China. The previous studies have discussed the factors that influence summer extreme precipitation in North China, and pointed out the possible impacts from WPSH and middle and high latitude circulations under global warming. However, we still have many problems need to be answered. How do North China extreme precipitations change in the 21st century, how the changes of extreme precipitations are connected with the changes of polar and subtropical circulation backgrounds? Why extreme precipitations occur on the weakening tendency of summer monsoon? Whether the WPSH and the middle and high latitude circulations have a combined influence on extreme precipitation The above questions need to be further explored.

This paper focus on the regional extreme precipitation in North China, and discuss the trend turning of extreme precipitations in July-August in North China. We explore how the changes of summer circulation over Eurasian continent and the WPSH influence extreme precipitation in North China in the early 21st century. Our study may shed a new light on the cause of extreme precipitation change in North China in the early 21st century. The data and analysis methods are presented in section 2. We analyze changes in extreme precipitation after 2003 in the section 3. Section 4 discusses Strengthening connection with Ural blocking after 2003. Section 5 discusses the strengthening connection with the WPSHI. Section 6 gives the conclusion and discussion.

2 Data And Method

2.1 Data

The data used in this study are the daily and monthly mean data in July and August from 1961–2020, they include: (1) the station-based observations of daily precipitation over the 107 stations in North China region (the 34.5°-44°N, 110°-123°E) from China's surface climate data set (V3.0) provided by the National Meteorological Information Center of China Meteorological Administration. (2) the daily and monthly sea level pressure, geopotential height, wind speed (u, v) and specific humidity at vertical 17 pressure levels from the National Centers for Environmental Prediction–National Center for Atmospheric Research (NCEP–NCAR) reanalysis data (Kalnay et al. 1996), (3) the monthly West Pacific Subtropical High Ridge Index and West Ridge Point Index from the National Meteorological Information Center of China Meteorological Administration. The monthly and daily climatologies are the averaging over the period 1961–2020.

2.2 Methods

A. Definition of regional extreme precipitation (REP) and normal precipitation (RNP) events

Percentile-based extreme precipitation index (Alexander et al. 2006) is defined at each station. For any station in North China, the wet day (precipitation > 0) precipitations from July to August from 1961 to 2020 are sorted from small to large, and the 95th percentile value is selected as the threshold. When the daily precipitation of a station exceeds the threshold, the day is defined as the extreme precipitation day for the station. The empirical orthogonal function (EOF) was performed on the normalized extreme precipitation days from July to August at all stations, and the variance contribution of the first mode (EOF1) is 13.78% (Fig. 1a). The EOF1 shows that the changes in extreme precipitation days in North China are regionally consistent, and the high-loading areas are distributed in the Beijing-Tianjin-Hebei and middle and lower reaches of the Yellow River. We selected a total of 68 stations at which the EOF1 is greater than 0.3 (big circles in Fig. 1a) as the representative stations of extreme precipitation in North China. A day when 1) at least 30% of the 68 representative stations have daily precipitation not less than 1 mm, and 2) at least 10% of the representative stations with daily precipitation exceeding the extreme precipitation threshold, is defined as a regional extreme precipitation (REP) day. Precipitation days that satisfy condition 1) but not satisfy condition 2) are defined as a regional normal precipitation (RNP) day. A consecutive precipitation day period with at least 1 REP day or a single REP day is defined as a REP event. A consecutive precipitation day period with only RNP days or a single RNP day is defined as a RNP event. The interval between two REP/RNP events must be 7 days or more, otherwise they are considered to be the same process. The first day of a REP/RNP event is defined as the Lag 0 day of a REP/RNP event.

B. Definition of the WPSHI index

The westward extending and northward lifting index of the WPSH (WPSHI) is defined based on the ridge line index and the western boundary index constructed by Liu et al. (2012), as follows.

$WPSHI_i = \frac{\left(D_i - \bar{D}\right)}{\sigma_D}, D_i = N_i - W_i, N_i = \frac{\left(a_i - \bar{a}\right)}{\sigma_a}, W_i = \frac{\left(b_i - \bar{b}\right)}{\sigma_b}$, where a_i and b_i are the ridge line index and the western boundary index of the WPSH respectively, i refers to each year. The monthly values of the ridge line indices and the western boundary indices from 1961–2020 are obtained from the National Climate Center (NCC) monitoring service (http://cmdp.ncc-cma.net/download/precipitation/diagnosis/NWP_high/wpsh_idx.txt). The$WPSHI$ reflects the yearly combined zonal and meridional variabilities of the WPSH over the western North Pacific (north of 10ºN, west of 150ºE).

C. Other methods used

We use running slope difference (RSD) t test (Zuo et al. 2019) with an 11-year window to detect trend turnings of the interanual variabilities of the REP frequency in the period 1961–2020. Rossby wave envelope propagation is analyzed using the wave activity flux defined by Takaya and Nakamura (2001). Background wave guide is evaluated by the Effective beta ($\beta_{\text{eff}} = \beta - \frac{\partial^2 U}{\partial y^2}$) (Hoskins and Karoly 1981). The baroclinicity is measured by the Eady Growth Rate (EGR) (Lindzen and Farrell 1980), which is calculated with the NCL function, eady_growth_rate (https://www.ncl.ucar.edu/Document/Functions/Contributed/eady_growth_rate.shtml). Characterization of elements such as circulation associated with REP events using composite methods.

According to the definition of Tibaldi and Molteni (1990), the daily blocking high index is calculated using the following scheme:

$$GHGS = \frac{Z(\varphi_0) - Z(\varphi_s)}{\varphi_0 - \varphi_s} \geq 0 \quad (2-1)$$

$$GHGN = \frac{Z(\varphi_N) - Z(\varphi_0)}{\varphi_N - \varphi_0} \leq -10 \quad (2-2)$$

where, $\varphi_N = 80^\circ N \pm \Delta$, $\varphi_0 = 60^\circ N \pm \Delta$, $\varphi_s = 40^\circ N \pm \Delta$, $\Delta = 0$or 5. According to the definition in Luo et al. (2016) and Zhang et al. (2018), we defined in this study an Ural High (UH) day when there is at least one longitude satisfying (2 – 1) and (2–2) within the range of 40°E-80°E. Moreover, a consecutive process with UH day no less than 5 days is defined as an Ural blocking (UB). The numbers of the UH days and the UB days are then counted respectively in the July-August in each year from 1961–2020.

3 Changes In Extreme Precipitation

3.1 REP trend turning and difference of REP characteristics between 1961–2002 and 2003–2020

According to the definition in section 2, the number of the REP days (REP frequency here after) and the intensity of REP (the mean daily precipitation averaging over all the REP days in July-August) in July-August is counted in each year from 1961 to 2020. The interannual variations of the normalized REP frequency and intensity time series are shown in Figs. 1b, 1c. Figure 1b shows that the interannual variabilities of the normalized REP frequency and the principle component corresponding to the EOF1 (PC1) of station-based extreme precipitation frequencies are nearly overlapped. This indicates that the REP event reflects a regional consistent extreme precipitation in North China represented by the pattern of the EOF1. The interannual correlation coefficient between the normalized REP frequencies and intensities is 0.97 (Fig. 1c), which indicates that the year with high REP frequency regularly corresponds the strong REP intensity. We use the REP frequency time series to show the interannual variability of the REP in the following analyses, which can be an indicator of the inter-annual variability of both the frequency and the intensity of the REP.

The RSD t test (Zuo et al. 2019) detected three trend turnings in the REP frequency time series of the period 1961–2020. They are 1986, 1995, and 2003 respectively (Fig. 1b). Though the varying linear trends extracted by the RSD t test appear to swing up and down, they are the linear part of the original oscillations of the time series. The REP frequencies in 1961–1984 show a decreasing trend, and the REP frequencies in 1985–1996 and in 1997–2002 show an increasing and then a decreasing trend afterward, so the overall trend of REP frequency in 1961–2002 is decreasing. In contrast, the REP frequency shows a significant increasing trend from 2003 to 2020. In this study, we aim to investigate the increase trend of the REP in 2003–2020, thus the period 1961–2002 of overall decrease trend is treated as a whole. So we divide the period 1961–2020 into two parts, one is 1961–2002 and the other is 2003–2020. In 1961–2002, the REP frequency has a weak negative correlation with the RNP frequency (Fig. 1d, black curve). However, the negative interannual correlation between the REP frequency and RNP frequency increases significantly from − 0.3 in 1961–2002 to -0.73 in 2003–2020. This indicates that the sharp increase in REP frequency is accompanied by a decrease in RNP frequency in North China after 2003, whereas the REP and RNP are relatively independent before 2003.

The trend turning around 2003 not only indicates the change of the linear trend in the two periods, it also indicates changes in other features of the REP. The spatial distributions of the extreme precipitation frequency before and after 2003 are shown in Figs. 1d and 1e. The larger July-August mean REP frequency in 1961–2002 is located nearly north of 37°N with an overall trend of decrease. The significant decrease trend is along a southwest-northeast direction belt from north of Shanxi province to west Liaoning province, and also over west Shandong province. But the larger July-August mean REP frequency shifts to a more southward region (south of 42°N) with a trend of increase in 2003–2020. The most significant increase exists over the lower reach of the Yellow River, the Beijing-Tianjin-Hebei region and west Liaoning province.

B. Typical circulation conditions corresponding to the REP in 1961–2002 and in 2003–2020

According to the REP events defined above, we obtained 78 and 31 REP events in 1961–2002 and 2003–2020, respectively. In order to reveal the circulation conditions at high and low levels of atmosphere and the corresponding water vapor transports, we composite 850 hPa water vapor transport vectors (qu, qv) and their divergence/convergence and the 200 hPa geopotential height anomalies at the Lag 0 day based on the REP events. The results are shown in Figs. 2a-f. As a comparison, we also composite the circulation and water vapor transport (Figs. 3a-f) based on RNP cases.

For both RNP and REP, the main moisture sources are at the Bay of Bengal and the South China Sea (Figs. 2a, d and 3a, d). Compared with RNP, the REP moisture transport and convergence are significantly enhanced. In 1961–2002, when the REP occurs, the location of the WPSH shows no significant anomaly and is basically consistent with the climatic mean. The airflows on the west side of the WPSH contribute little to the water vapor transport of the REP. This means that REP is not closely related to the day-to-day variation of WPSH. However, in 2003–2020, the WPSH is significantly strengthened at Lag 0 day, and the 5880 gpm contour extends westward to the lower reaches of the Yangtze River (Figs. 2a, d), which leads to a stronger moisture transport from south China sea and an extra moisture transport from the northern west Pacific to North China (Figs. 2a, d). Although the composite circulations corresponding to the RNP also show that the subtropical high in 2003–2020 expands more northward and westward than that in 1961–2002, its western boundary is located along the east China coast. Thus the WPSH circulation during the RNP has very small impact on the moisture transport during the RNP (Figs. 3a, d). So, we have a conclude that in 2003–2020, the expanding of the WPSH to the lower reaches of the Yangtze River makes it to be a significant impact on REP.

According to Fig. 2 and Fig. 3, the patterns of circulation and moisture transport corresponding to the REP are obviously different from those corresponding to RNP for both the period 1961–2002 and 2003–2020. Comparing Figs. 2b, e and 3b, e the composite anomalies of the 850 hPa moisture transport vector show that the difference between REP and RNP lies in the strong cyclonic circulation over North China on the Lag 0 day and the strengthened anti-cyclonic circulation over the region from northeast China to the Japan Sea. The southwesterly flow between the cyclone and the anticyclone is significantly enhanced, thereby enhancing the transport and convergence of water vapor from the Bay of Bengal and the South China Sea to North China. However, the 850 hPa moisture transport anomaly field on the RNP only shows that there is a weak cyclonic circulation over North China. At 200 hPa, both REP and RNP are accompanied by a structure of low pressure on the west and high pressure on the east of North China. The 200 hPa low pressure is located mainly at Mongolia (ML, hereafter), and the high pressure is located over northeast China and the Korean Peninsula (NEH, hereafter). Therefore, the low pressure and high pressure (the low-high dipole) are located on the northwest side of the 850 hPa cyclone and anticyclone, respectively. This constitutes a typical baroclinic structure. So, air rising exists at the east side of the 200 hPa low pressure center (Figs. 2c, e and 3c, e). However, the NEH corresponding on the Lag 0 day of the REP events is increased significantly, and the divergent west of the NEH is strong. Thus, the vertical velocity reached more than 5 times that corresponding to the RNP (Figs. 2c, 2f, and 3c, 3f). Therefore, the strong upward movement and abundant water vapor caused the extreme precipitation in North China.

Moreover, compared with that in 1961–2002, there are significant changes in the circulations corresponding to the REP in 2003–2020. The composite results show that the low-high dipole associated with REP are located in the subtropical jet near 40˚N, the subtropical wave train is significant, whereas, the geopotential height anomalies over the subpolar region near 60 ˚N are weak in 1961–2002 (Fig. 2c). However, the 200 hPa composite circulations corresponding to the REP in 2003–2020 show that the geopotential height anomalies over the subpolar region are strengthened significantly. Specifically, a high pressure anomaly exists over the Ural Mountains region (the UH), the ML is located more northward, at a location away from the subtropical jet area, and the NEH is located more southwestward (Fig. 2f). Thus, in 2003–2020, the 200 hPa low-high dipole and the corresponding 850 hpa cyclone-anticyclone pair show a clockwise tilting of the axis of the low-high dipole when comparing to that in 1961–2002(Figs. 2b, 2c, 2e, 2f). With the cooperation of the westward expanding WPSH, the 850 hPa anticyclone circulation expands southwestward (Figs. 2a, 2b, 2d, 2e). As a result, the low-level moisture convergence belt in 2003–2020 is located more southward and extends more westward than it is in 1961–2002 (Figs. 2a, 2b, 2d, 2e). In other words, in 1961–2002, the moisture convergence belt is mainly located in the northern part of North China, whereas in 2003–2020 the moisture convergence belt lies in the southern part of North China, that is, the lower reaches of the Yellow River and the Beijing-Tianjing-Hebei region.

For the RNP, the corresponding composite 200 hPa geopotential height anomaly field at Lag 0 is dominated by a more typical Silk Road Pattern (Kosaka et al. 2013) in the subtropical jet region in 1961–2002 (Fig. 3e). Whereas, the composite 200 hPa circulations at Lag 0 of the RNP events in 2003–2020 showed a significant enhancement of the subpolar wave train and a weakening of the subtropical wave train, a change in the two Eurasian zonal wave trains that is similar to the case related to the REP events in 2003–2020 (Fig. 3f). Although the RNP events in 1961–2002 are accompanied by a similar low-high dipole as that related to the REP events, the eastern high pressure is much weaker, and the location of the low-high dipole is more eastward. In 2003–2020, the composite 200 hPa circulation at Lag 0 of the RNP events is dominated by a large-scale Mongolian low, and a much weaker high pressure located east of the Korean Peninsula. The anomalies of the RNP 850 hPa moisture transport vector field only show a strengthened northerly flow on the west side of the cyclone. Therefore, the southerly flow and moisture transport during RNP is much weaker than that of REP. Moreover, the vertical velocity related to the RNP is much weaker than that in the case of the REP (Figs. 3c, 3f). In summary, the significant enhancement of the upper level NEH is a key mid-latitude local circulation feature that distinguishes REP from RNP.

4 Possible Reasons For Change Of The Rep

4.1 Strengthening connection with Ural blocking after 2003

A. Low-high dipole amplified by upstream Rossby wave activity

The above composite analysis indicates that one of the most significant features of the circulation corresponding to the REP is the amplification of the NEH in the upper troposphere. In order to explore the cause of the NEH development, the composite daily evolution of the circulations one week before the Lag

0 day of the REP events is shown in Fig. 4. For both in 1961–2002 and in 2003–2020, the composite daily evolution of the circulation corresponding to the REP shows the following common features. One week before the occurrence of REP, a mid-latitude high pressure anomaly exists near 120ºE as a precursor of the NEH. From Lag − 7 to Lag 0, the Rossby wave activity fluxes distributed zonally along a path across the Eurasian continent (Fig. 4 and Fig. 5) indicates an eastward Rossby wave energy propagation and leads to a continuous growth of the ML and the NEH. At Lag 0 the ML and the NEH reach the strongest (Figs. 4 and 5) and compose an amplified upper level low-high dipole. In addition, during the development of the low-high dipole from Lag − 7 day to Lag 0 day, the positions of the centers of the zonal wave train are geographically stable, showing a quasi-stationary wave pattern. As a comparison, during the daily evolution of the circulations corresponding to the RNP, we find a similar eastward propagating Rossby wave energy and a formation of low-high dipole structure at Lag 0. However, the action centers of the wave train move along the westerly jet, which leads to a much weaker and travelling wave pattern, thus results in a weaker low-high dipole (Figs. 6 and 7). The above analysis shows that the occurrence of REP is accompanied by the preexisting high pressure anomaly near 120ºE and a quasi-stationary wave train over Eurasian continent. The eastward propagation of Rossby wave energy along the wave train leads to a persistent growing of the stable low-high dipole and finally forms a strongly amplified one.

Comparing the two periods before and after 2003, we further found that in 1961–2002 the Rossby wave activity flux that accompanies the development of the low-high dipole of the REP mainly distributed along the subtropical wave train. The amplified low-high dipole at Lag 0 shows a zonal distribution along the subtropical jet. Though the evolution of the NEH is accompanied by the UH persists at northern Ural, there is no significant wave energy connection between this subpolar region high and the NEH (Fig. 4). However, in 2003–2020, the UH exists at central and southern Ural before the occurrence of the REP. From Lag − 7 to Lag 0, a large part of Rossby wave activity flux propagates northeastward and leads to a continuous strengthening of the UH. With the gradual strengthening of the UH (from Lag − 6 day), the wave energy propagating along the subtropical weakens significantly. Due to the persistent growth of the UH, there is a stronger Rossby wave energy propagating southeastward from the UH, and the ML strengthens significantly. As a result, the low-high dipole related to the REP becomes more meridional in 2003–2020 than that in 1961–2002. In summary, the enhancement of low-high dipole before the occurrence of the REP is a result of the eastward propagation of upstream Rossby wave energy along the subtropical/polar waveguide in 1961–2002/2003–2020. But the low-high dipole is more zonal/meridional in 1961–2002/2003–2020.

The composite sub-seasonal evolution of the wave trains corresponding to the RNP also shows a significant enhancement of the subpolar wave train in 2003–2020. However, the wave activity flux that leads to the amplification of the low-high dipole corresponding to the RNP is along the subtropical wave guide both in 1961–2002 and in 2003–2020.

B. Connection between the UH and the NEH and impacting of background circulation

The composite daily evolutions of the REP events show that the local low-high dipole are connected with the daily evolutions of upper level wave trains over Eurasia Continent. In order to show the background circulation for the daily evolution of the wave trains, we regress the July-August mean 200 hPa geopotential height anomaly field to the yearly REP frequency time series. The common features of the stationary waves for high REP frequency years (the REP years, hereafter) in both 1961–2002 and 2003–2020 are the existence of a strong stationary high geopotential height anomaly with its center over northeast China (the northeast ridge, hereafter) (Figs. 8a, b). However, the stationary wave patterns upstream of the northeast ridge are much different between those in 1961–2002 and in 2003–2020. In 1961–2002, the high geopotential height anomaly with its center east of the Caspian Sea and the northeast ridge construct a typical Circumglobal Teleconnection (CGT) (Ding and Wang 2005). And the subtropical Asian westerly jet is located between the low geopotential height anomaly with its center located at the south of the Ural Mountains and the high geopotential height anomaly east of the Caspian Sea, a background pattern that leads to a stronger westerly jet. However, in 2003–2020, the subtropical stationary wave pattern is different from the CGT pattern, which shows a low geopotential height anomaly east of the Caspian Sea accompanying the northeast ridge. The south of the Ural Mountains is dominated by a strong stationary high geopotential height anomaly (the Ural ridge, hereafter) which is opposite to the circulation in 1961–2002. Thus the subtropical jet is weakened as it is located at south of the Ural ridge. Moreover, in 2003–2020 the northeast ridge is stronger and located more southwestward than that in 1961–2002. And the amplitudes of the stationary waves along the polar region are larger in the period 2003–2020 than those in the period 1961–2002.

As a comparison, the July-August 200hPa geopotential height anomaly fields that regressed to the yearly RNP frequency time series (Figs. 6 and 7) show that the region that is dominated by the northeast ridge in the REP years is covered by a low geopotential height anomaly in the high RNP frequency years both in 1961–2002 and in 2003–2020. The stationary wave patterns corresponding to high RNP frequency years also show an enhancement of geopotential height anomaly along north coast of Eurasian continent in 2003–2020 comparing to that in 1961–2002. However, the Ural region is dominated by a low geopotential height anomaly in high RNP frequency years for both of the two periods. So, the background stationary wave pattern corresponding to the RNP years is almost opposite to that in high REP frequency years, especially over northeast China. Therefore, the stationary northeast ridge is a characteristic feature of the background circulation of high REP frequency years. Considering the results in Figs. 4–7, it can be seen that the distributions of the stationary wave in high REP/RNP frequency years are similar to the circulations one week before the REP or RNP. This indicates that the seasonal background stationary waves provide a background and preconditions for the development of the daily circulation of the REP/RNP.

The above discussion indicates that the circulations that leads to the REP develop from a typical background stationary wave pattern with a preexisting background northeast ridge. To further investigate how the background condition influence the daily variation of the circulation corresponding to the REP, we analyze the dynamic features of the background field. The correlation coefficients of the July-August averaged 200 hPa zonal wind field, 200 hPa background effective beta (waveguide) and 300 hPa Eady

growth rate (EGR)with the time series of the yearly REP frequency of both the periods 1961–2002 and 2003–2020 are calculated and shown in Fig. 9. The effective beta ($\beta_{\text{eff}} = \beta - \frac{\partial^2 U}{\partial y^2}$) (Hoskins and Karoly 1981) reflects the beta effect of background westerlies. If zonal jet is strong enough, it acts as a waveguide for Rossby wave (Hoskins and Ambrizzi 1993). The EGR is a measure of basic flow baroclinic instability (Lindzen and Farrell 1980).

For the two periods 1961–2002 and 2003–2020, the regressed distribution of background zonal winds is consistent with the distribution of the background stationary waves. In 1961–2002, the westerly wind speed, westerly waveguide and the EGR are very weak along the polar front, but are strong over subtropical jet for the REP years. Therefore, Rossby waves are less active in the polar front regions, but more active along the subtropical jet. In 2003–2020, the distinguish change in the stationary wave pattern is the significant enhancement of the Ural ridge. As a result, for the REP years, the regressed zonal wind, the EGR and the westerly wave guide show significant enhancements north of the Ural ridge from northern Europe to Siberia (Fig. 9), which means a strengthening of Rosbby wave activity. Meanwhile, the westerly wind speed, the westerly wave guide and the EGR along the subtropical jet are weakened for the REP years, indicating a weaker Rossby waves activities.

In 2003–2020, the regression results show that the pre-existing stationary ridge (Fig. 8) and the weakened westerly wind over the south of the Ural Mountains region (Figs. 9d-f) provide favorable conditions for the development of atmospheric blockings (Shutts 1983; Berckmans et al. 2013; Luo et al. 2014) in the REP years. In the Downstream of the Ural stationary ridge, the polar front waveguide turns southeastward near 90˚E, and extends to northeast China via Lake Baikal, along which the westerly wind and the EGR is also large. This is beneficial for development and the propagating of Rossby waves along this path. And it is confirmed by the composite results of the daily evolution fields (Fig. 4) which shows a wave train from the Arctic to northeast Asia forms during the development of the REP circulations. It is a bridge that links the UH and the NEH.

For the period 1961–2002, the regressed July-August mean 200 hPa zonal wind field shows a similar weakened westerly wind region near 60˚N (Figs. 9a-c) in the REP years. However, it is located at a much higher latitude, which is consistent with the regressed stationary ridge at the north of the Ural Mountains. This background conditions are also benefit for the occurrence of atmospheric blockings in the REP years. We can see from the composite daily evolution of the circulations before the REP in the period 1961–2002 that a persistent positive geopotential height anomaly accompanies the development process of the REP circulation. However, there is no significant wave activity propagation from the high anomaly at the north of the Ural Mountains to the NEH. Thus the linkage between the two high anomalies is weak.

The above results indicate that it is the enhancement of the polar stationary wave and the existence of the stationary southern Ural ridge that provide a background condition leading to the change of wave energy propagation path from along the subtropical westerly jet in 1961–2002 to the polar front in 2003–2020 (Fig. 5) and constructer a linkage between the UH and the NEH. To verify the above speculation, we

calculated the interannual variation of yearly July-August UH days and the Ural blocking days (Fig. 10). In this study we define the persistent UH that lasts for no less than 5 days as a Ural blocking and count the blocking days (UB). Our result also shows that the UH days almost equal to the UB days, which indicates that the existence of an UH day means an occurrence of a blocking event. The correlation between the UB days and the REP frequency has no statistical significance in 1961–2002 but it is significantly enhanced in 2003–2020 (Fig. 10). This result confirms the above analysis that the linkage between the REP and the Ural blockings appears in 2003–2020 due to the enhancement of the southern Ural stationary ridge and the change of Rossby wave propagation path.

4.2 Strengthening connection to the WPSH

To further analyze the connection between the WPSH and the REP, we composite the Lag − 7 day to Lag 0 day evolution of the 5880 gpm geopotential height contour which represents the spatial distribution of the WPSH, based on the REP/RNP cases, and also composite the July-August mean 5880 gpm geopotential height contour based on the REP/RNP years (the year in which the detrended REP/RNP frequency anomalies greater than 0.5 variance) for the periods of both 1961–2002 and 2003–2020 (Fig. 11).

The daily evolutions of the 5880 gpm contours corresponding to the REP and the RNP in1961-2002 and the REP in 2003–2020 show a westward extending and then an eastward retreating (Figs. 11a-d) from Lag − 7 day to Lag 0 day. Since the east-west swing of the 5880 gpm contours occurs mostly in the western Pacific Ocean (Figs. 11a, c, d), the WPSH has very small contribution to the water vapor transport anomaly during the occurrence of REP/RNP in 1961–2002 and the RNP in 2003–2020 (Lag 0 day) (Figs. 2b and 3b, e). As shown by the composite REP circulation, though the REP in 1961–2002 is not influenced by the WPSH, the moisture transport is strengthened by the NEH. The above mentioned daily variabilities of the 5880 gpm contour are consistent with the pattern of the July-August mean 5880 gpm contours corresponding to the REP and RNP years in 1961–2002 and RNP year in 2003–2020, whose western edge are located at east of or near 130ºE.

Whereas, in 2003–2020, the composite 5880 gpm contour corresponding to the REP continue to move westward and northward especially in the period from Lag − 4 to Lag 0 day. This is different from the REP cases in 1961–2002 and the RNP cases in the both periods. On Lag 0 day, the west edge of the 5880 contour is located at the middle and lower reaches of the Yangtze River (Figs. 11b and 2d), enhancing the water vapor transport from the western Pacific and the South China Sea to North China (Figs. 2d, e). Therefore, the 2003–2020 REP events are significantly associated with the daily variations of the WPSH due to its contribution to moisture transport. On the other hand, earlier studies found that the intraseasonal west-east shift of the subtropical high is connected to the propagation of the stationary Rossby waves along the Asian Jet in the upper troposphere (Tao and Wei 2005; Enomoto et al. 2003; Dong and He 2020). Comparing the daily evolutions of the composite 200 hPa circulations (Fig. 5) and the composite 5880 gpm contour corresponding to the 2003–2020 REP events (Fig. 11b) from Lag − 4 day to Lag 0 day, we can find that the daily variation of the WPSH is closely related to the development of

the NEH which is a result of the Rossby wave activity propagation along the polar wave train. From Lag − 4 day to Lag 0 day of REP, the 200 hPa NEH extends to the Japan Sea and intensifies gradually (Fig. 11b). However, before the Lag − 4 day, the NEH is located more westward thus it has almost no impact on the WPSH. For the period 2003–2020, the westward expanding July-August mean WPSH corresponding to the REP year locates near the Japan Sea (Fig. 11e) which is much more westward than that in REP years in 1961–2002 and in the RNP years. The WPSH can be influenced by the upper-troposphere NEH, because the subsidence on the southeast side of the NEH (Figs. 2c-d) contributes to the strengthening of the low-level high pressure over west Northern Pacific. As a result, the westward and northward expanded background WPSH in 2003–2020 provides a precondition for a further continuously westward and northward extending of the daily WPSH as the 200 hPa NEH continues to expand eastward and strengthen before the REP. The connection between the NEH and the WPSH is thus formed.

The inter-annual variability of the WPSHI (the westward-northward expanding index of the WPSH defined in section 2) shows that there is no significant trend in WPSHI in the period 1961–2002. However, in 2003–2020 it shows an increase trend (Fig. 12), indicating that the WPSH extends westward and northward after 2003. This is consistent with the composite results shown in Fig. 11. Though the WPSHI and REP frequency are generally positively correlated in both periods of 1961–2002 and 2003–2020, the correlation between the WPSHI and REP frequency is not significant in 1961–2002. This confirm the result that the WPSH has little impact on the REP in the period 1961–2002 because it is located more eastward far from the east coast of Asian continent. However, in 2003–2020, the correlation between the WPSHI and the REP frequency increases significantly, especially after 2007, the interannual variation of WPSHI is almost consistent with the interannual variation of REP frequency. It confirms the enhancing impact of the WPSH on the REP in 2003–2020 when the WPSH expanding more westward and northward. As a conclusion, the connection between the WPSH and the REP in 2003–2020 arises from the below two conditions. First, the strong westward and northward expanding of the WPSH results in an extra moisture transport from the west Northern Pacific and South China Sea adding to the moisture transport from the Bay of Bengal which strengthens the total moisture supply to the REP in North China. Second, the forming of connection between the daily evolutions of the upper troposphere NEH and the WPSH when the mean WPSH expands to west of 130ºE. Moreover, the enhanced connection between the WPSH and the REP and the increase trend of the WPSHI may explain the increase of the strength and frequency of the REP in 2003–2020.

5 Conclusion And Discussions

5.1 Conclusion

Based on the July-August REP events and RNP events distinguished in the period 1961–2020, we explore the trend turning and the corresponding changes of the REP in North China during July-August and its relationship with Ural blockings and the WPSH. The frequency and intensity of the REP in North China turned from a weak decrease trend in 1961–2002 to a significant increase trend in 2003–2020. The REP

frequency increased significantly in Beijing-Tianjin-Hebei region, the middle and lower reaches of the Yellow River and the western Liaoning province, which means a southward shift of REP after 2003.

Through a comparison between the circulations and moisture transports corresponding to the REP events and those corresponding to the RNP events, we show the critical circulation conditions that leads to the REP in North China, and explain how it changes and leads to a trend turning around 2003, which is manifested by a schematic diagram in Fig. 13. The REP in North China is characterized by a strongly amplification of upper troposphere low-high dipole with their center near Mongolia (ML) and Northeast China (NEH) respectively, which reinforces local air rising and northward moisture transports. The amplified upper level low-high dipole leads to a strong enhancement of lower level southerly flow between the low level cyclonic-anti-cyclonic pair, which further transports the moisture brought by summer monsoon circulation and the WPSH from Bay of Bengal and western north Pacific to North China, and leads to a strong amplification of moisture convergence and precipitation there. For the REP both in 1961–2002 and in 2003–2020, the daily variation and enhancement of NEH stems from the following two conditions. First, in the REP year, there is a background stationary ridge over the northeast China (the northeast ridge). Second, the eastward propagating of Rossby wave energy along the polar wave guide or the subtropical wave guide reinforce the preexisting northeast ridge, so that it develops into a NEH and leads to REP in North China.

Obvious differences of the circulations corresponding to the REP exist between the period 1961–2002 and the period 2003–2020. The first difference lies in the middle and high latitudes zonal wave trains. In 1961–2002, the NEH is amplified by the upstream wave energy propagating along the subtropical wave train, since the polar wave guide is very weak. Whereas, in 2003–2020, the existence of the stationary Ural ridge provides background conditions for the formation of Ural blockings and the existence of a northwest-southeastward wave train linking the Ural blocking and the NEH. Therefore, the NEH is amplified by the wave energy propagation along the polar wave train. The correlation between the REP frequency and the Ural blocking is then significantly enhanced in 2003–2020. The shift of wave propagation path from along the subtropical wave guide in 1961–2002 to along the polar wave guide in 2003–2020 results in a strengthened-and- northeastward-shift/southwestward-shift of the low/high of the LHD, with a corresponding clockwise tilt of the moisture transport path in 2003–2020 compared to 1961–2002. The second difference lies in the WPSH. In 1961–2002, the west edge of the WPSH corresponding to the REP years is located east of 130°E, so its contribution to the moisture transport to North China is weak. The summer monsoon circulation act as the major moisture source for the REP. Therefore, the correlation between REP frequency and the WPSH is very weak in 1961–2002. In 2003–2020, the July-August mean WPSH corresponding to the REP year expands westward and northward, and the 5880 gpm contour expands to west of 130°E and lifts northward to near 35°N, which is located very near to the upper level stationary northeast China ridge. Correspondingly, the daily WPSH continues to extend northward and westward to the middle and lower reaches of the Yangtze River under the influence of the continuous enhancement of the 200 hPa NEH during the developing stage of the REP events (Lag − 7 day to Lag 0 day). Therefore, the southeasterly flow on the western edge of the WPSH brings additional moisture besides those transported by the monsoon southwesterly flow, thereby enhancing

moisture transport during the REP. Moreover, under the combined influence of the NEH and the WPSH, the moisture convergence belt (rain belt) shifts southward and extends westward. Correspondingly, REP rain belt has a southward shift, and extreme precipitation intensifies in the middle and lower reaches of the Yellow River, Beijing-Tianjin-Hebei and western Liaoning province in 2003–2020. And the interannual correlation between the WPSH and REP is also enhanced in 2003–2020 (Fig. 12). Thus, due to the significant correlation between the REP and the WPSHI in 2003–2020, the increasing trend of WPSHI (Fig. 12, continuously westward and northward expanding of the WPSH) implies stronger extra moisture supply from the north western Pacific, which can partly explain the increase and enhancement of REP in 2003–2020. Moreover, the enhanced linkage of the REP to the Ural blocking is another possible reason for the increase of the extreme precipitation in North China, since blockings are a major source of persistent circulation anomaly.

5.2 Discussions

The results in this study found that both in 1961–2002 and in 2003–2020, moisture transported by summer monsoon circulation is the major moisture source for extreme precipitation in North China. This is consistent with the previous studies (Ding and Chan 2005; Huang et al. 2006; Liu and Ding 2011). Therefore, the northward advance and southward withdrawal of summer monsoon are consistent with the movements of extreme precipitation (He et al. 2020; Cui et al. 2018). However, this study further indicated that extreme precipitations are also impacted by the midlatitude NEH or the low-high dipole located over west and east of North China, which is a direct local circulation condition that reinforce moisture transport and air rising thus leads to extreme rains. Because, the NEH is amplified majorly by the two zonal wave trains over the Eurasian continent, to some extent, extreme precipitations can occur when the summer monsoon is weak. So this may explains the result pointed out by Zhou et al. (2013) that the 2012 flood in North China occurred in the context of a multidecadal drying tendency. As for the connection with the WPSH, this study found that the westward and northward expanding of the WPSH in 2003–2020 brings extra moisture from the western north Pacific thus lead to a stronger extreme rain than that in 1961–2002 when the WPSH is located more eastward. This is consistent with the recent findings that the intensifying of the WPSH since 2000s leads to a northward stretching of the front rain belt and a reinforcing of precipitations in North China (Han et al. 2020; Chen and Zhang 2020). However, this study shows some new findings. The intensification and expanding of the July-August mean WPSH in 2003–2020 provides a precondition for a further westward and northward expanding under the influence of the intra-seasonal developing of the upper level NEH. The inland expanding WPSH together with the southward tilted upper level low-high dipole modulates the path of the low level westerly jet and results in a southward shift and westward extending of the extreme rain belt. Moreover, this study further shows that the extreme precipitations in North China changes from a weak connection with the WPSH in 1961–2002 to a significant connection in 2003–2020. This may explain the increase of extreme precipitations in the recent two decades (Li et al. 2013; Zhao et al. 2019), since the WPSH shows an intensifying trend (Choi and Kim 2019; Fu and Guo 2020).

This study not only shows what the circulation corresponding to the REP is, but also explains what cause the amplification of the local circulation that leads to extreme precipitations. The circulation pattern of the REP found in this study is consistent with Zhao et al. (2019). They also shown the extreme precipitation is accompanied by a strengthened southwesterly or southeasterly low level jet and low pressure anomalies at west of North China. In this study, we further showed that the amplification of the low-high dipole that leads to the REP is a result of both preexisting northeast stationary ridge and downstream propagation of Rossby wave energy along the polar front or subtropical jet. Thus, our study confirm the results pointed by Orsolini et al. (2015) and Gao et al. (2022) that North China extreme precipitations are connected with midlatitude wave trains. And this study also confirms the result of Yang et al. (2021) that extreme precipitation is accompanied by July-August mean anticyclone over the Korean Peninsula after the 1970s. Beyond the results that consistent with the earlier research indicated above, this study further found that accompanying the trend turning of REP days from a decrease in 1961–2002 to an increase in 2003–2020, the connection between the Ural blocking and the REP in North China becomes significant in 2003–2020. As for the generation of the Ural blocking, Liu et al. (2022) attribute it to positive summer shortwave cloud radiative anomalies over northern Russia. Nakamura and Sato (2022) pointed out that East Asian rainfall is being enhanced by high-latitude atmospheric circulations due to the Arctic warming. Thus the strengthening connection between the Ural blocking and the REP may indicate a connection between Arctic change and extreme precipitation in North China. This needs to further study in future.

Declarations

Acknowledgements

This work was jointly sponsored by the National Natural Science Foundation of China (NSFC) Projects (42075025), National Key Basic Research Project of China (Grant 2019YFA0607002), Shandong Natural Science Foundation Project (ZR2019ZD12), Taishan Pandeng Scholar Project, the open fund of State Key Laboratory of Satellite Ocean Environment Dynamics, Second Institute of Oceanography, Ministry of Natural Resources (QNHX2217).

Funds

This work was jointly sponsored by the National Natural Science Foundation of China (NSFC) Projects (42075025), National Key Basic Research Project of China (Grant 2019YFA0607002), Shandong Natural Science Foundation Project (ZR2019ZD12), the open fund of State Key Laboratory of Satellite Ocean Environment Dynamics, Second Institute of Oceanography, Ministry of Natural Resources (QNHX2217).

Date availability

Station-based observations of daily precipitation over the 107 stations in North China region (the 34.5°-44°N, 110°-123°E) from China's surface climate data set (V3.0) were provided by the National Meteorological Information Center of China Meteorological Administration. (http://data.cma.cn/data/cdcdetail/dataCode/A.0012.0001.html), NCEP/NCAR datasets were obtained from https://psl.noaa.gov/data/gridded/data.ncep.reanalysis.html; The monthly values of the ridge line indices and the western boundary indices from 1961-2020 are obtained from the National Climate Center (NCC) monitoring service (http://cmdp.ncc-cma.net/download/precipitation/diagnosis/NWP_high/wpsh_idx.txt).

Competing interests

I declare that the authors have no competing interests as defined by Springer, or other interests that might be perceived to influence the results and discussion reported in this paper.

Authors' contributions

Yina Diao, Jinghuan Guo, and Yazhou Zhang contributed to the conceptualization and design of the study. Figures visualization and formal analysis were performed by Jinghuan Guo and Yina Diao. The first draft of the manuscript was written by Yina Diao, and all authors reviewed and approved the manuscript.

References

1. Alexander LV, Coauthors, (2006) Global observed changes in daily climate extremes of temperature and precipitation. J Geophys Res 111:D05109. https://doi.org/:10.1029/2005JD006290
2. Antokhina OY, Antokhin PN, Martynova YV, Mordvinov VI (2016) The impact of atmospheric blocking on spatial distributions of summertime precipitation over Eurasia. IOP Conf Ser: Earth Environ Sci 48:012035. https://doi.org/10.1088/1755-1315/48/1/012035
3. Berckmans J, Woollings T, Demory ME, Vidale PL, Roberts M (2013) Atmospheric blocking in a high resolution climate model: influences of mean state, orography and eddy forcing. Atmos Sci Lett 14(1):34-40. https://doi.org/10.1002/asl2.412
4. Chen Z, Zhang J (2020) The characteristics of late summer extreme precipitation in northern China and associated large-scale circulations. Int J Climatol 40(12):5170-5187. https://doi.org/10.1002/joc.6512
5. Choi W, Kim KY (2019) Summertime variability of the western North Pacific subtropical high and its synoptic influences on the East Asian weather. Sci Rep 9:7865. https://doi.org/10.1038/s41598-019-44414-w
6. Cui DY, Wang CH, Santisirisomboon J (2019) Characteristics of extreme precipitation over eastern Asia and its possible connections with Asian summer monsoon activity. Int J Climatol 39:711-723. https://doi.org/10.1002/joc.5837

7. Ding QH, Wang B (2005) Circumglobal Teleconnection in the Northern Hemisphere Summer. J Clim 18(17):3483-3505. https://doi.org/10.1175/JCLI3473.1
8. Ding QH, Wang B (2007) Intraseasonal Teleconnection between the Summer Eurasian Wave Train and the Indian Monsoon. J Clim 20(15):3751-3767. https://doi.org/10.1175/JCLI4221.1
9. Ding YH, Chan JCL (2005) The East Asian summer monsoon: an overview. Meteorol Atmos Phys 89:117-142. https://doi.org/10.1007/s00703-005-0125-z
10. Dong X, He C (2020) Zonal displacement of the Western North Pacific subtropical high from early to late summer. Int J Climatol 40(11):5029-5041. https://doi.org/10.1002/joc.6508
11. Enomoto T (2004) Interannual Variability of the Bonin High Associated with the Propagation of Rossby Waves along the Asian Jet. J Meteor Soc Japan 82(4):1019-1034. https://doi.org/10.2151/jmsj.2004.1019
12. Enomoto T, Hoskins BJ, Matsuda Y (2003) The formation mechanism of the Bonin high in August. QJR Meteorol Soc 129:157-178. https://doi.org/10.1256/qj.01.211
13. Fu YH, Guo D (2020) Projected changes in the western North Pacific subtropical high under six global warming targets. Atmos Oceanic Sci Lett 13(01):26-33. https://doi.org/10.1080/16742834.2020.1696649
14. Gao H, Jiang W, Li WJ (2014) Changed relationships between the East Asian summer monsoon circulations and the summer rainfall in eastern China. J Meteorol Res 28:1075-1084. https://doi.org/10.1007/s13351-014-4327-5
15. Gao YX, Hsu PC, Che SJ, Yu CW, Han SR (2022) Origins of Intraseasonal Precipitation Variability over North China in the Rainy Season. J Clim 35(18):6219-6236. https://doi.org/10.1175/JCLI-D-21-0832.1
16. Gong DY, He XZ (2002) Interdecadal change in western Pacific subtropical high and climatic effects. Acta Geographica Sinica 57(2):185-193.
17. Han TT, Guo XY, Zhou BT, Hao X (2020) Recent Changes in Heavy Precipitation Events in Northern Central China and Associated Atmospheric Circulation. Asia-Pacific J Atmos Sci 57:301-310. https://doi.org/10.1007/s13143-020-00195-1
18. Han TT, Zhang MH, Zhu JW, Zhou BT, Li SF (2021) Impact of early spring sea ice in Barents Sea on midsummer rainfall distribution at Northeast China. Clim Dyn 57:1023-1037. https://doi.org/10.1007/s00382-021-05754-4
19. He LQ, Hao X, Li H, Han TT (2021) How do extreme summer precipitation events over eastern China subregions change? Geophy Res Lett 48:e2020GL091849. https://doi. org/10.1029/2020GL091849.
20. He SP, Gao YQ, Furevik T, Wang HJ, Li F (2018) Teleconnection between Sea Ice in the Barents Sea in June and the Silk Road, Pacific–Japan and East Asian Rainfall Patterns in August. Adv Atmos Sci 35:52-64. https://doi.org/10.1007/s00376-017-7029-y.
21. Hoskins BJ, Ambrizzi T (1993) Rossby Wave Propagation on a Realistic Longitudinally Varying Flow. J Atmos Sci 50(12):1661-1671. https://doi.org/10.1175/1520-0469(1993)050<1661:RWPOAR>2.0.CO;2

22. Hoskins BJ, Karoly DJ (1981) The Steady Linear Response of a Spherical Atmosphere to Thermal and Orographic Forcing. J Atmos Sci 38(6):1179-1196. https://doi.org/10.1175/1520-0469(1981)038<1179:TSLROA>2.0.CO;2
23. Huang RH, Chen JL, Huang G, Zhang QL (2006) The Quasi-Biennial Oscillation of Summer Monsoon Rainfall in China and Its Cause. Chin J Atmos Sci 30(4):545-560.
24. Kalnay E, Coauthors, (1996) The NCEP/NCAR 40-Year Reanalysis Project. Bull Am Meteorol Soc 77(3):437-472. https://doi.org/10.1175/1520-0477(1996)077<0437:TNYRP>2.0.CO;2
25. Kosaka Y, Nakamura H, Watanabe M, Kimoto M (2009) Analysis on the Dynamics of a Wave-like Teleconnection Pattern along the Summertime Asian Jet Based on a Reanalysis Dataset and Climate Model Simulations. J Meteor Soc Japan 87(3):561-580. https://doi.org/10.2151/jmsj.87.561
26. Kosaka Y, Xie SP, Lau NC, and Vecchi GA (2013) Origin of seasonal predictability for summer climate over the Northwestern Pacific. Proceedings of the National Academy of Sciences, 110(19): 7574-7579.
27. Kwok R, Cunningham GF, Wensnahan M, Rigor I, Zwally HJ, Yi D (2009) Thinning and volume loss of the Arctic Ocean sea ice cover: 2003-2008. J Geophys Res 114:C07005. https://doi.org/10.1029/2009JC005312
28. Li JP, Ren RC, Qi YQ, Wang FM, Lu RY, Zhang PQ, Jiang JH, Duan WS, Yu F, Yang YZ (2013) Progress in air-land-sea interactions in Asia and their role in global and Asian climate change. Chinese J Atmos Sci 37(2):518-538. https://doi.org/10.3878/j.issn.1006-9895.2012.12322
29. Li JP, Zeng QC (2003) A new monsoon index and the geographical distribution of the global monsoons. Adv Atmos Sci 20(2):299-302. https://doi.org/10.1007/s00376-003-0016-5
30. Lindzen RS, Farrell B (1980) A simple approximate result for the maximum growth rate of baroclinic instabilities. J Atmos Sci 37:1648-1654.
31. Liu HW, Ding YH (2011) The interdecadal variability of summer precipitation over North China. J Appl Meteorol Sci 22(02):129-137.
32. Liu L, Wu B, Ding S (2022) On the association of the summertime shortwave cloud radiative effect in northern Russia with atmospheric circulation and climate over East Asia. Geophys Res Lett 49:e2021GL096606. https://doi.org/10.1029/2021GL096606
33. Liu YY, Li WJ, Ai WX, Li QQ (2012) Reconstruction and application of the monthly western Pacific subtropical high indices. J Appl Meteorol Sci 23(4):414-423.
34. Luo DH, Cha J, Zhong LH, Dai AG (2014) A nonlinear multiscale interaction model for atmospheric blocking: The eddy-blocking matching mechanism. QJR. Meteorol Soc 140:1785-1808. https://doi.org/10.1002/qj.2337
35. Luo DH, Xiao YQ, Yao Y, Dai AG, Simmonds I, Franzke CLE (2016) Impact of Ural Blocking on Winter Warm Arctic-Cold Eurasian Anomalies. Part I: Blocking-Induced Amplification. J Clim 29(11):3925-3947. https://doi.org/10.1175/JCLI-D-15-0611.1
36. Maslanik J, Stroeve J, Fowler C, Emery W (2011) Distribution and trends in Arctic sea ice age through spring 2011. Geophys Res Lett 38:L13502. https://doi.org/10.1029/2011GL047735

37. Matsumura S, Sugimoto S, Sato T (2015) Recent Intensification of the Western Pacific Subtropical High Associated with the East Asian Summer Monsoon. J Clim 28(7):2873-2883. https://doi.org/10.1175/JCLI-D-14-00569.1
38. Nakamura T, Sato T (2022) A possible linkage of Eurasian heat wave and East Asian heavy rainfall in Relation to the Rapid Arctic warming. Environ Res 209:112881. https://doi.org/10.1016/j.envres.2022.112881
39. Orsolini YJ, Zhang L, Peters DHW, Fraedrich K, Zhu X, Schneidereit A, van den Hurk B (2015) Extreme precipitation events over north China in August 2010 and their link to eastward-propagating wave-trains across Eurasia: observations and monthly forecasting. QJR Meteorol Soc 141:3097-3105. https://doi.org/10.1002/qj.2594
40. Schubert SD, Wang HL, Koster RD, Suarez MJ, Groisman PY (2014) Northern Eurasian Heat Waves and Droughts. J Clim 27(9):3169-3207. https://doi.org/10.1175/JCLI-D-13-00360.1
41. Shutts GJ (1983) The propagation of eddies in diffluent jetstreams: eddy vorticity forcing of 'blocking' flow fields. QJR Meteorol Soc 109:731-161. https://doi.org/10.1002/qj.49710946204
42. Takaya K, Nakamura H (2001) A formulation of a phase-independent wave-activity flux for stationary and migratory quasigeostrophic eddies on a zonally varying basic flow. J Atmos Sci 58:608-627. https://doi.org/10.1175/1520-0469(2001)058<0608:AFOAPI>2.0.CO;2
43. Tao SY, Wei J (2006) The westward, northward advance of the subtropical high over the West Pacific in summer. J Appl Meteorol Sci 17(5):513-525
44. Tibaldi S, Molteni F (1990) On the operational predictability of blocking. Tellus A 42:343-365. https://doi.org/10.1034/j.1600-0870.1990.t01-2-00003.x
45. Wang HJ (2001) The Weakening of the Asian Monsoon Circulation after the End of 1970's. Adv Atmos Sci 18(3):376-386. https://doi.org/10.1007/BF02919316
46. Wang WP, Zhang ZQ, Xu YJ, Xiang Y (2015) Characteristics of the precipitation concentration period in China. Acta Meteor Sinica 73(6):1052-1065. https://doi.org/10.11676/qxxb2005.078
47. Xu ZQ, Fan K, Wang HJ (2015) Decadal Variation of Summer Precipitation over China and Associated Atmospheric Circulation after the Late 1990s. J Clim 28(10):4086-4106. https://doi.org/10.1175/JCLI-D-14-00464.1
48. Yang L, Zhao JH, Li S, Zang NH, Feng GL (2021) Enhanced impact of early-summer tropical eastern Pacific sea surface temperature on the July-August precipitation over North China after the late 1970s. Int J Climatol 42:3463-3476. https://doi.org/10.1002/joc.7427
49. Yu RC, Zhou TJ (2007) Seasonality and Three-Dimensional Structure of Interdecadal Change in the East Asian Monsoon. J Clim 20(21):5344-5355. https://doi.org/10.1175/2007JCLI1559.1
50. Yu RC, Wang B, Zhou TJ (2004) Tropospheric cooling and summer monsoon weakening trend over East Asia. Geophys Res Lett 31:L22212. https://doi.org/10.1029/2004GL021270
51. Zhang QY (1999) The variations of the precipitation and water resources in North China since 1880. Plateau Meteorol 18(4):486-495.

52. Zhang RN, Sun CH, Zhang RH, Jia LW, Li WJ (2018) The impact of Arctic sea ice on the inter-annual variations of summer Ural blocking. Int J Climatol 38(12):4632-4650. https://doi.org/10.1002/joc.5731
53. Zhao Y, Xu XD, Li J, Zhang R, Kang YZ, Huang WB, Xia Y, Liu D, Sun XY (2019) The large-scale circulation patterns responsible for extreme precipitation over the North China plain in mid-summer. J Geophys Res: Atmos 124:12794-12809. https://doi.org/10.1029/ 2019JD030583
54. Zhou TJ, Gong DY, Li J, Li B (2009) Detecting and understanding the multi-decadal variability of the East Asian summer monsoon-Recent progress and state of affairs. Meteor Z 18:455-467. https://doi.org/10.1127/0941-2948/2009/0396.
55. Zhou TJ, Song FF, Lin RP, Chen XL, Chen XY (2013) The 2012 North China floods: explaining an extreme rainfall event in the context of a long-term drying tendency. Explaining extreme events of 2012 from a climate perspective. Bull Am Meteorol Soc 94(9):S49-S51. https://www.researchgate.net/publication/298701648
56. Zhou X, Sun JS, Zhang LN, Chen JG, Cao J, Ji B (2020) Classification characteristics of continuous extreme rainfall events in North China. Acta Meteor Sinica 78(5):761-777. https://doi.org/10.11676/qxxb2020.052
57. Zhu KF, Xue M (2016) Evaluation of WRF-based convection-permitting multi-physics ensemble forecasts over China for an extreme rainfall event on 21 July 2012 in Beijing. Adv Atmos Sci 33:1240–1258. https://doi.org/10.1007/s00376-016-6202-z
58. Zhu YL, Wang HJ, Zhou W, Ma JH (2011) Recent changes in the summer precipitation pattern in East China and the background circulation. Clim Dyn 36:1463-1473. https://doi.org/10.1007/s00382-010-0852-9
59. Zuo B, Li JP, Sun C, Zhou X (2019) A new statistical method for detecting trend turning. Theor Appl Climatol 138:201-213. https://doi.org/10.1007/s00704-019-02817-9

Figures

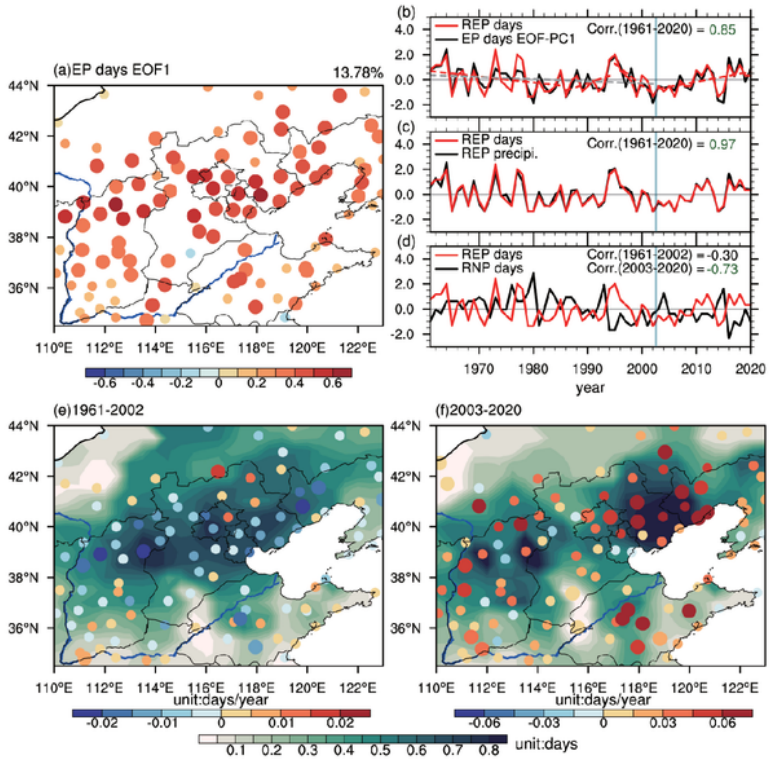

Fig. 1 (a) The first EOF (EOF1) of July-August extreme precipitation days at each station in North China from 1961 to 2020, (b) the corresponding PC of the EOF1 (black curve), the yearly REP days (red curve), and the trends of the yearly REP days (red dashed lines, with detection parameter T = 11years, confidence level at 90%) and their turnings (break point of the dashed red lines), (c) yearly REP days (red curve) and yearly precipitation averaging over all the REP day in July-August (black curve), (d) yearly REP days (red curve) and RNP days(black curve), (e-f) spatial distributions the average (color shading) and trend (dot) of the station based extreme precipitation frequencies in 1961-2002 (e) and 2003-2020 (f) respectively. Detrended correlation coefficients between two time series in (b-d) are denoted at top right corners in each subfigure with the green number being statically significant at the 95% level, the gray dashed line in (b) denotes the total trend of REP days in period 1961-2002, the vertical blue line denotes the turning point at 2003, large dots in (e-f) indicate the 90% confidence level.

Figure 1

See image above for figure legend

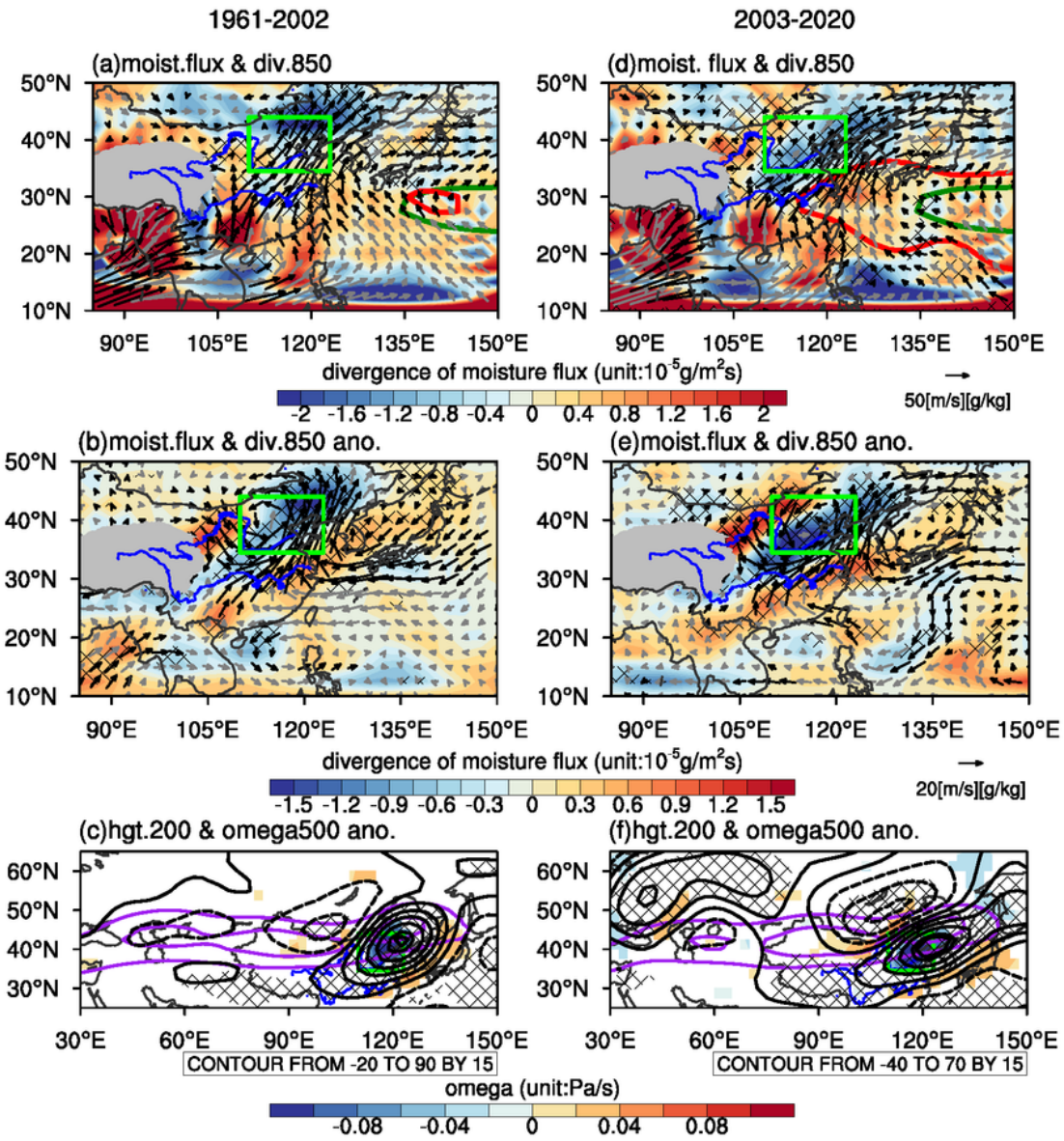

Fig. 2 Composites of the original values (a, d) and the anomalies (b, e) of moisture transport vector (black arrow) and moisture transport divergence (color shading) at 850 hPa, and 200 hPa geopotential height anomalies (contour) and vertical velocity anomalies (Pa/s, color shading, only values exceeding 90% confidence level are shown) (c, f) at the Lag 0 day, based on all the REP events in 1961-2002 (a, b, c) and 2003-2020 (d, e, f) respectively. The red and green contours in (a, d) are the composite the 5880 gpm contour (denoting the spatial distribution of the WPSH) at the Lag 0 day and the climatology of July-August mean 5880 gpm contour respectively, and the purple contour in (c, f) are zonal wind velocity that are larger than 20m/s, grey crossing in (a, d, c, f) denote statistical significance larger than 90%, gray shading denotes the Tibet Plateau (elevations above 3,000 m).

Figure 2

See image above for figure legend

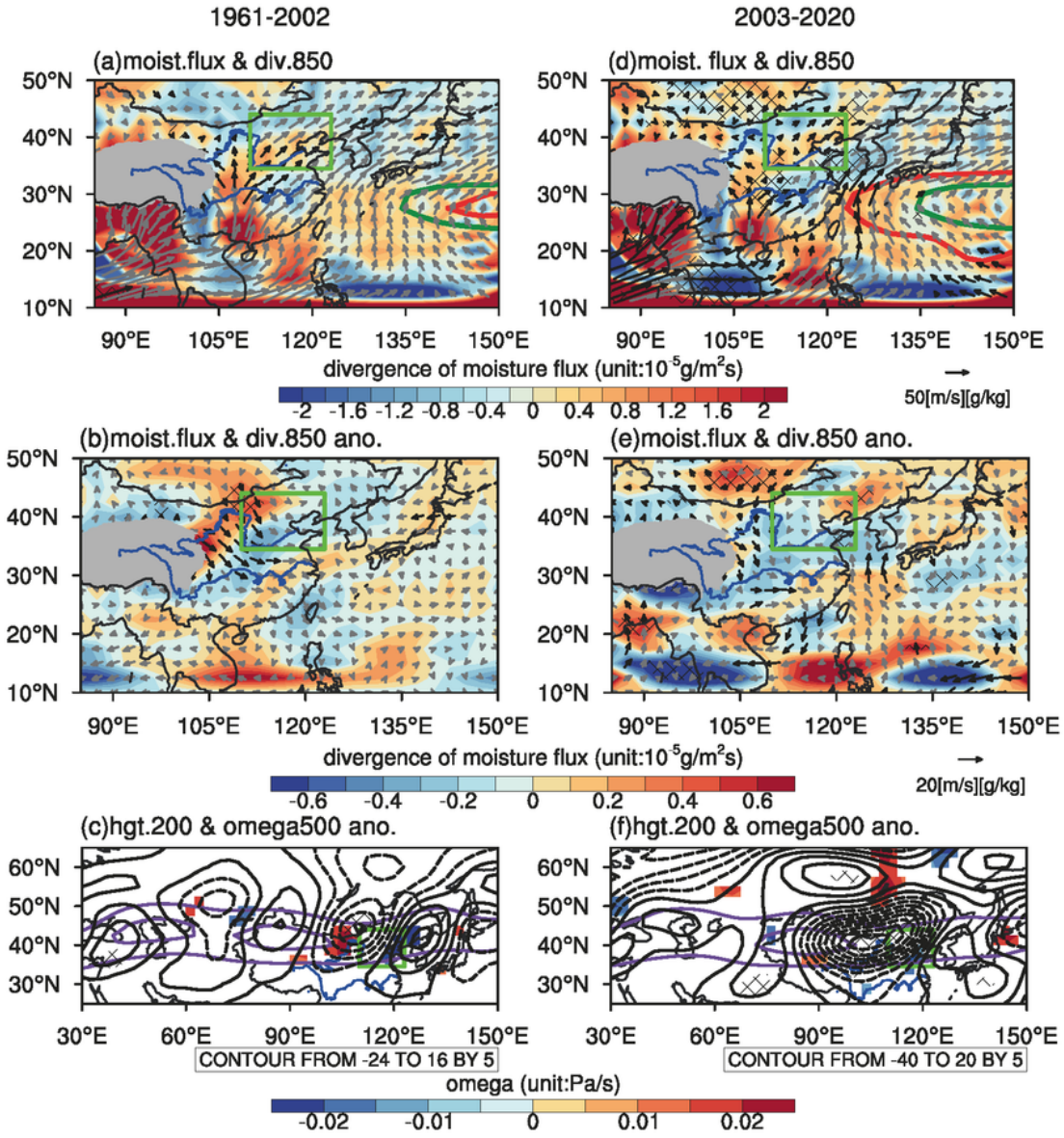

Fig. 3 As in Fig. 2, but for the RNP events.

Figure 3

See image above for figure legend

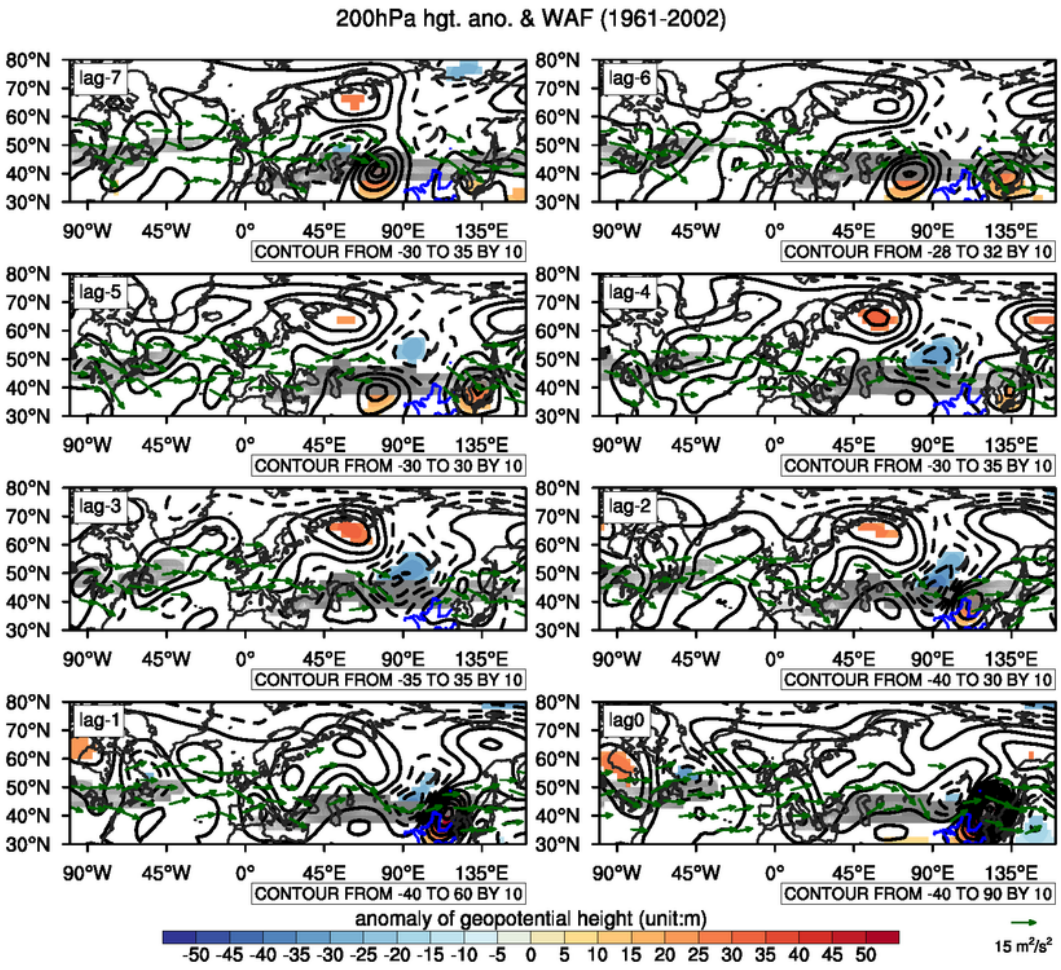

Fig. 4 Composites of geopotential height anomalies and wave activity flux vectors at 200 hPa from Lag -7 day to Lag 0 day, based on all the REP events in period 1961-2002, color shading denote composite geopotential height anomalies that exceed 90% confidence level.

Figure 4

See image above for figure legend

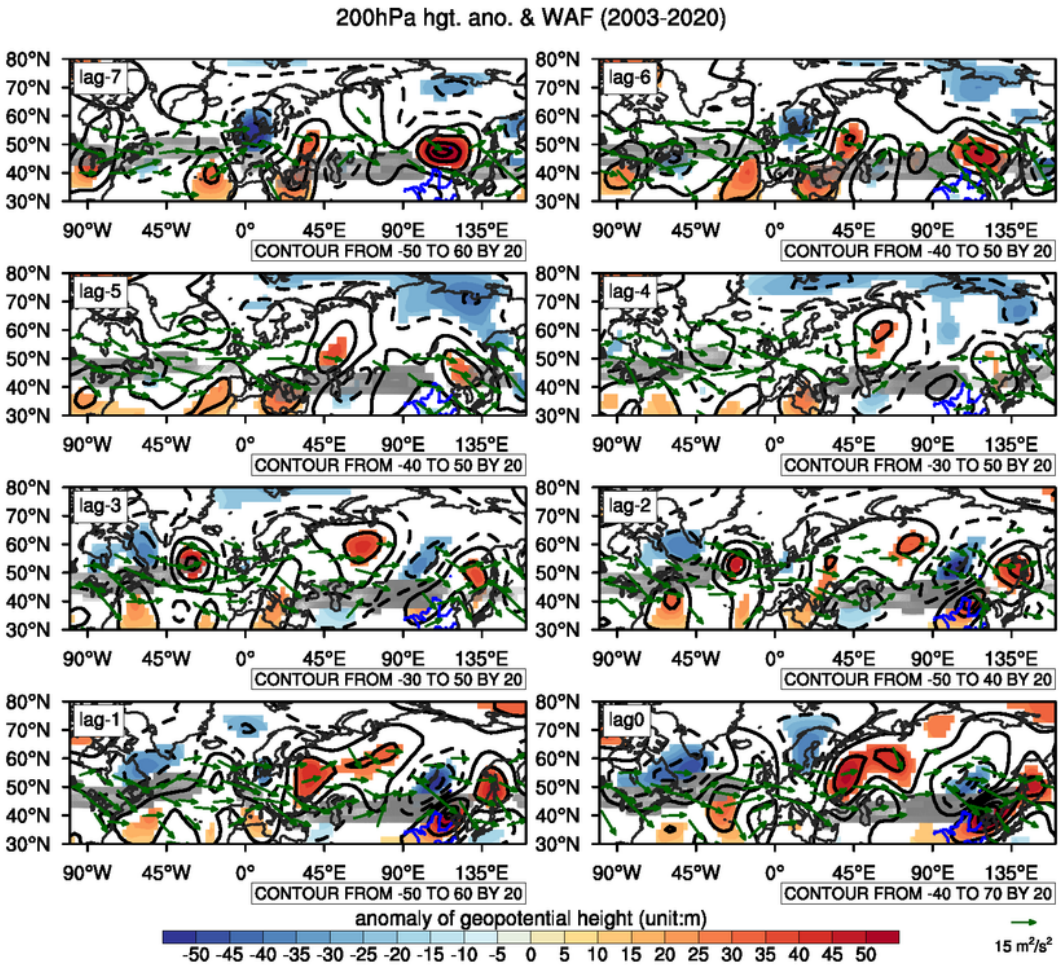

Fig. 5 As in Fig. 4, but for the REP events in the period 2003-2020.

Figure 5

See image above for figure legend

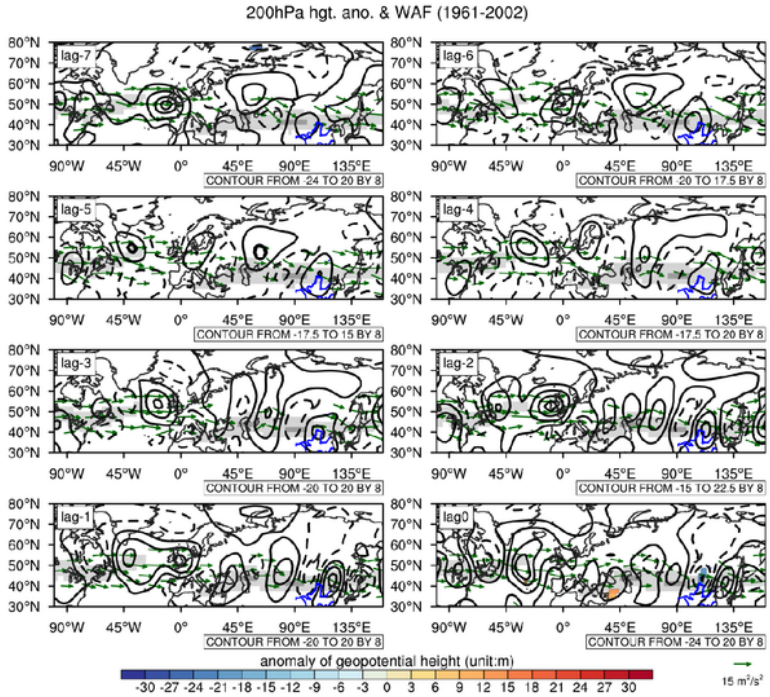

Figure 6. As in Figure 4, but for the RNP events in the period 1961-2002.

Figure 6

See image above for figure legend

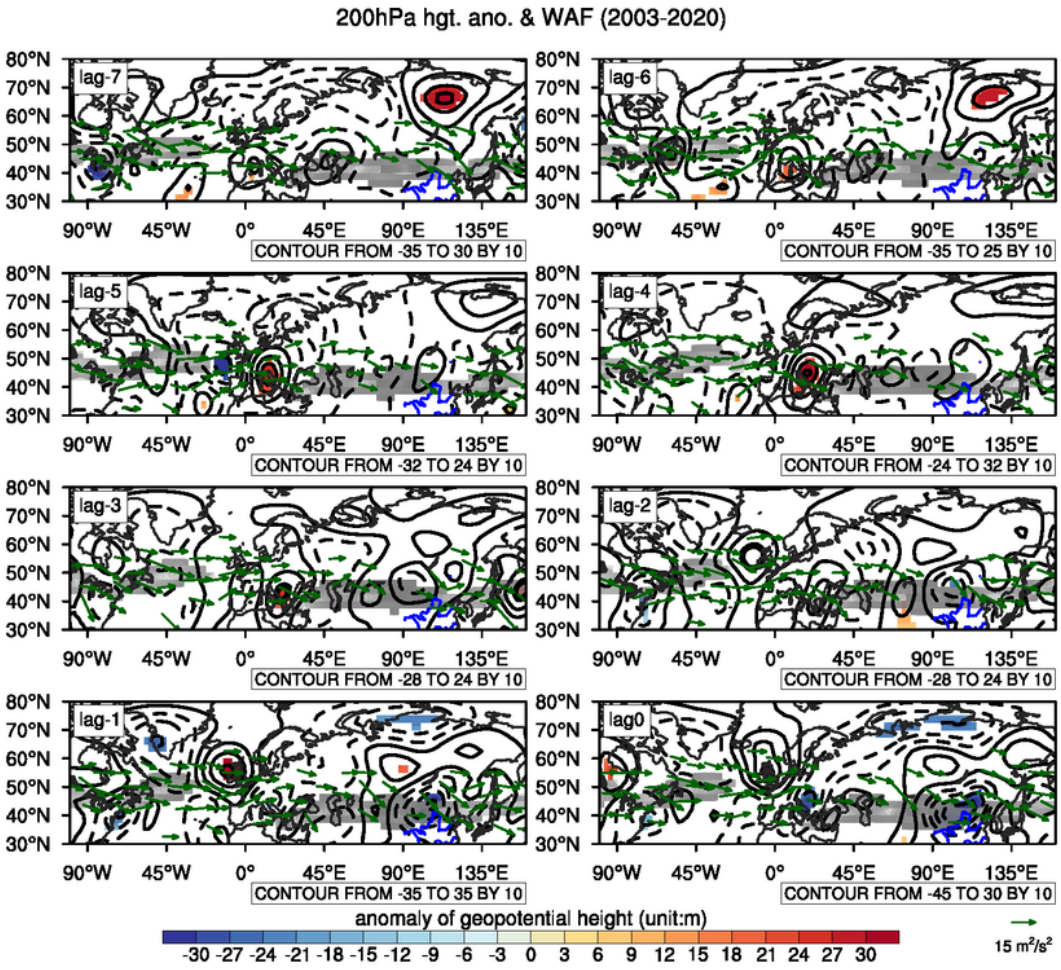

Fig. 7 As in Fig. 4, but for the RNP events in the period 2003-2020.

Figure 7

See image above for figure legend

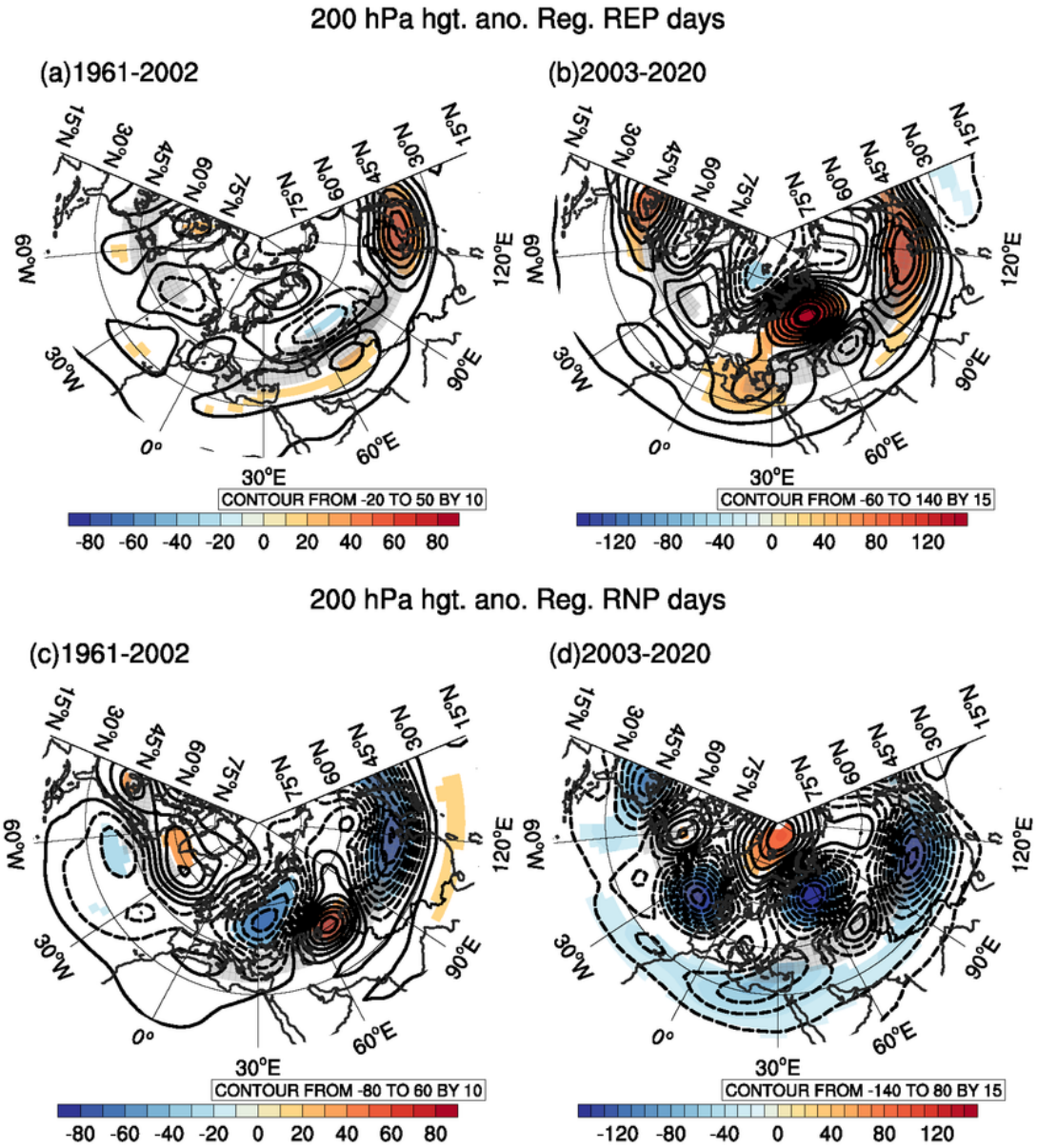

Fig. 8 Regression of July-August mean 200 hPa geopotential anomalies (contours) to the inter-annual variabilities of the REP days (a, b) and RNP days (c, d) respectively, in the period 1961-2002 (a, c) and the period 2003-2020 (b, d), the color shading denotes the regressed value with statistical significance larger than 90%, the gray shading denotes the July-August mean zonal wind velocity, both the 200 hPa geopotential anomalies and the inter-annual variation of the REP days are detrended.

Figure 8

See image above for figure legend

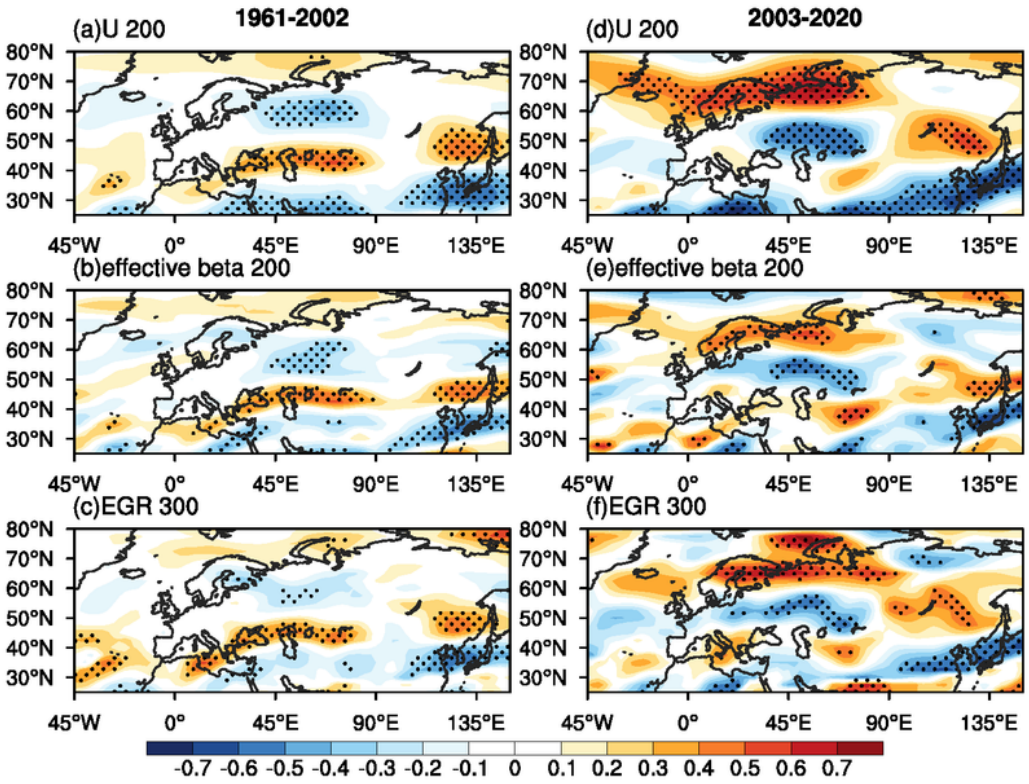

Fig. 9 Correlations between the REP days and the July-August mean 200 hPa zonal wind (U) velocity (a, d), 200hPa effective beta (b, e), and 300 hPa Eady growth rate (c, f) respectively in the period 1961-2002 (a-c) and the period 2003-2020 (d-f), black dots denote statistical significance larger than 90%.

Figure 9

See image above for figure legend

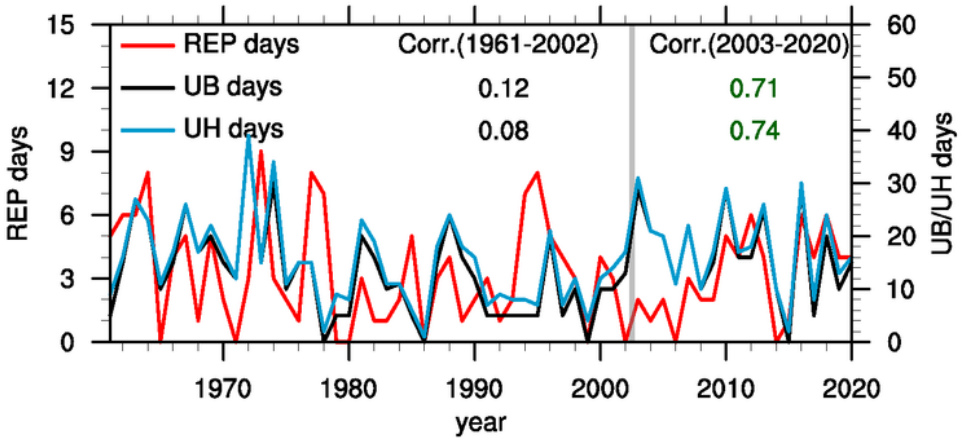

Fig. 10 Inter-annual variabilities of the REP days (red curve), the Ural high days (blue curve), the Ural blocking days (black curve), the vertical gray line denotes the trend turning point at 2003, the numbers denote the correlation coefficients, with the green number denotes the 95% confidential level.

Figure 10

See image above for figure legend

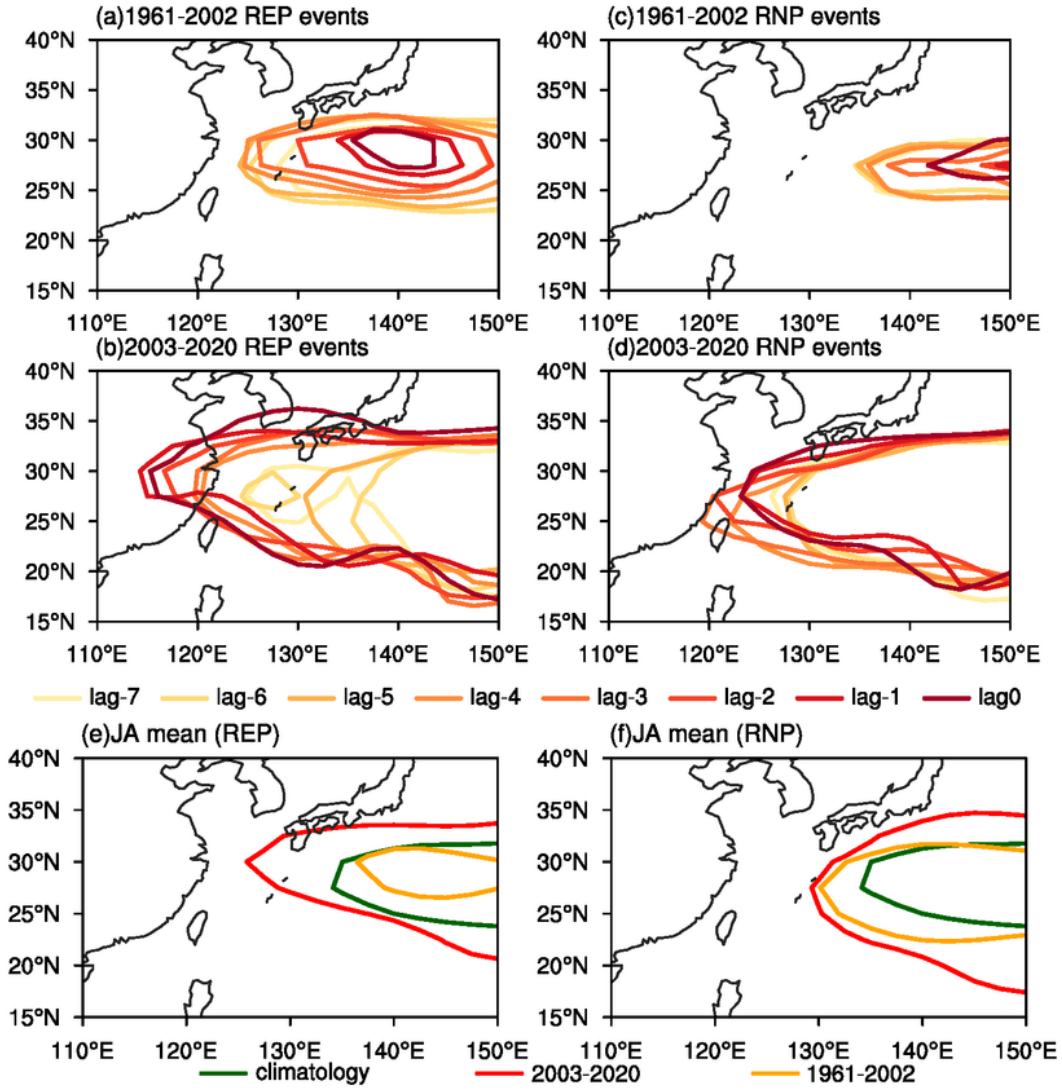

Fig. 11. Composite daily variabilities of the 5880 gpm contours from Lag-7 to Lag 0 based on the (a) REP and (b) RNP events in 1961-2002, and (c) REP and (d) RNP events in 2003-2020, and composite July-August mean 5880 gpm contours based on the (e)REP and (f) RNP years in 1961-2002 (yellow contour) and 2003-2020 (red contour) and the climatology of the 5880 gpm contour (green, averaging over the period 1961-2020).

Figure 11

See image above for figure legend

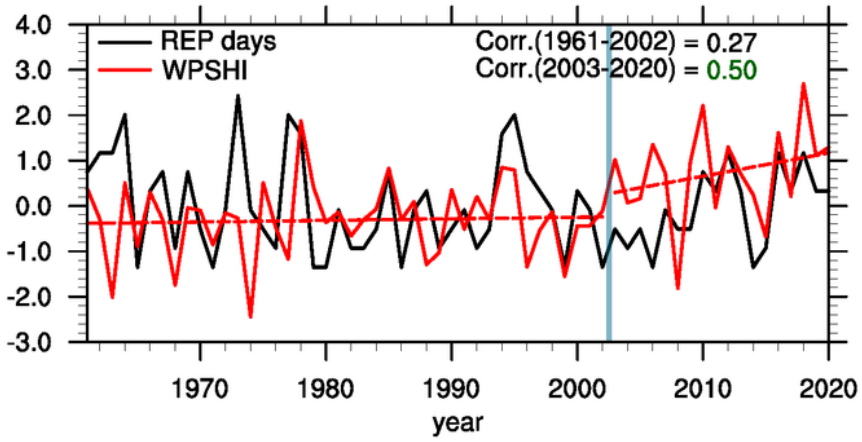

Fig. 12 Inter-annual variabilities of normalized REP days (black curve) and WPSHI (red curve) respectively, the red dashed lines denote trends of the WPSHI in 1961-2002 and 2003-2020 respectively, the green number denotes the correlation coefficient exceeds 95% confidence level.

Figure 12

See image above for figure legend

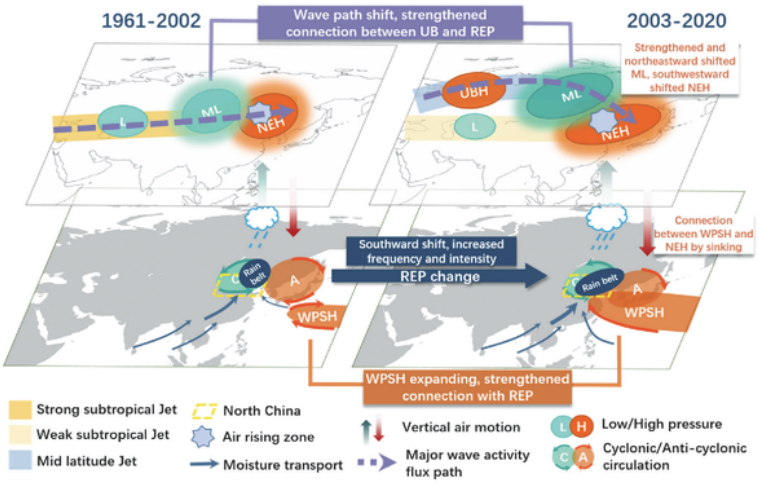

Fig. 13 Schematic diagram explains how the REP changes from the period 1961-2002 to the period 2003-2020 and why its connections with Ural blocking (UB) and the western Pacific Subtropical high (WPSH) are enhanced in 2003-2020.

Figure 13

See image above for figure legend